J Fail. Anal. and Preven. (2009) 9:159–170
DOI 10.1007/s11668-009-9212-7

TECHNICAL ARTICLE—PEER-REVIEWED

Creep and Fatigue Failure in Single- and Double Hot Arm MEMS Thermal Actuators

Nasim Paryab · Hamid Jahed · Amir Khajepour

Submitted: 18 November 2008 / Published online: 13 February 2009
© ASM International 2009

Abstract Determination of the failure mechanisms of mechanical devices is the key to the design of reliable products. This paper reports an investigation on creep and fatigue failure of microelectromechanical (MEMS) thermal actuators. Finite element modeling is used to predict thermomechanical behavior of actuators under low to moderate voltage differences. The modeling results are compared with experimental results to evaluate the models. Two probable failure modes associated with thermal actuators, that is, fatigue and creep, are investigated, and it is found that creep is the dominant failure mechanism. The creep behaviors of several U-shape and double hot arm thermal MEMS actuators are examined, and their deformation-time curves are obtained numerically and experimentally. The curves follow a typical three-stage creep curve usually observed in metals. The creep life cycles of the devices are compared on the basis of their stress and temperature distributions. This study shows that actuators with the maximum temperature occurring at the location where the high stress is induced have shorter life spans than those experiencing the high stress away from the maximum temperature location. It is concluded that the double hot arm actuators with equal length have longer creep life than the U-shape (single hot arm) actuators.

Keywords Creep · Creep failure · Failure mechanism · Fatigue failure

N. Paryab · H. Jahed (✉) · A. Khajepour
Mechanical and Mechatronics Engineering, University of Waterloo, Waterloo, ON N2L3G1, Canada
e-mail: hjahedmo@uwaterloo.ca

Introduction

Microelectromechanical system (MEMS) actuators enable MEMS devices to interact with their environment and are categorized based on their actuation sources into four main groups: electrostatic, electromagnetic, piezoelectric, and electrothermal actuators. The idea of using thermal expansion in MEMS actuators was first proposed by Guckel et al. [1] in 1992 and was later implemented by Comtois and Bright [2] and developed as a practical MEMS device by Burns and Bright [3]. Among thermal actuators, flexural actuators are being widely used in MEMS applications because of their fabrication characteristics. They can be fabricated using most of the surface micromachining processes and can be operated in integrated circuit (IC) device voltage and power ranges. Long-term performance is the major concern with ongoing applications of thermal actuators [4]. Developing a reliable MEMS actuator makes it cost effective and saves repair, reproduction, or even redesign time. An accurate failure model can lead to a safe and reliable design.

The operational conditions of thermal actuators keep them under high temperatures and stresses and make creep a viable mode of failure for these actuators. Stress and temperature distributions are important factors in the creep life cycle. On the other hand, as thermal actuators work mostly as on/off switches, fatigue becomes another possible failure mechanism of thermal actuators. The maximum stress level determination is important in fatigue study. Flexural thermal actuators have different design and operational conditions. The structure and the applied voltage levels have significant influence on the operational stress and temperature distributions in flexural thermal actuators.

The MEMS thermal actuators are primarily fabricated from polysilicon, which is a brittle material that becomes ductile after the transient temperature (813, 933 K [5], or between 923 and 1023 K [6]). Teh and Lin [7] were the first to address "the time-dependent deformation phenomenon of thin films under compressive stress" or "creeplike behavior" of polysilicon. Until now, high-temperature permanent deformation [6, 8, 9] and creep failure [4, 5, 7, 10, 11] of polysilicon microdevices have been reported by several research groups. Tuck et al. [5] reported that high temperature has a larger effect on creep behavior than high stress and that temperature is a very important variable in causing strain.

There have also been a number of fatigue studies on micropolysilicon samples and devices under electrostatic loading (Brown et al. [12] and Muhlstein et al. [13]) and electromechanical loading (Conant and Muller [4], Comtois et al. [14], Kapels et al. [15], Que et al. [16] Chen et al. [17, 18], Hocheng et al. [19], and Kung and Chen [20]). Some of these research works were related to the flexural thermal actuators [2, 4, 14, 15, 20]. Kung and Chen [20] reported fatigue failure of thermal actuators and fitted the empirical fatigue equations to the experimental data. Conant and Muller [4] rejected the fatigue failure and indicated that the failure is a time- and temperature-dependent failure. Ritchie et al. [21], Muhlstein et al. [13], Alsem et al. [22], and Kahn et al. [23] did extensive studies on the cause of fatigue failure and factors influencing its occurrence in polysilicon.

In this study, a comprehensive finite element modeling (FEM) process of the device is introduced. The model is validated based on experiments performed on several U-shape thermal actuators (single hot arm). Different experiments are performed on single and double hot arm thermal actuators. The stress and temperature distributions in the actuators and the effect of their distributions on the creep and fatigue life of the devices are discussed in detail. It is shown that fatigue is not a feasible failure mechanism in the thermal actuators studied in this work and that creep is both a viable and dominant failure mechanism.

Thermal Actuators Finite Element Modeling

A typical U-shape flexural thermal actuator consists of two arms (a narrow hot arm and a wider cold arm) that are connected at one end (via) and anchored to the substrate at the other ends (Fig. 1). Applied electrical current flows through the actuator via anchors, and the narrower arm (hot arm) becomes hotter than the wider arm (cold arm) as a result of ohmic resistance differences. This, in turn, causes a larger thermal expansion in the hot arm, and hence the actuator deflects toward the cold arm in an arc-shape motion.

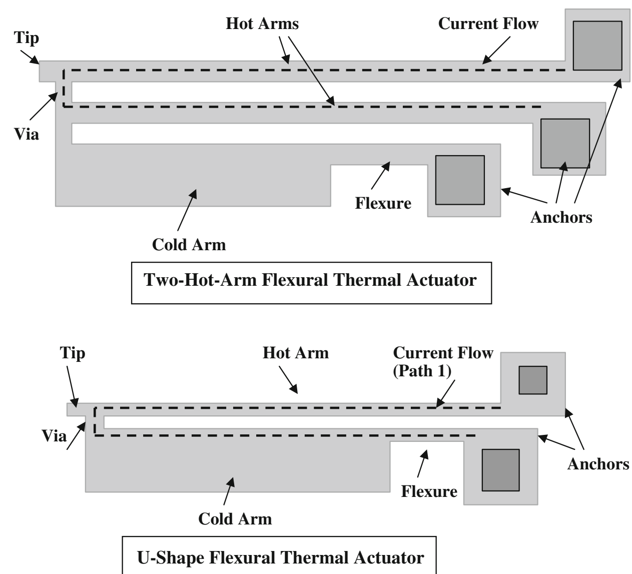

Fig. 1 Double hot arm and U-shape flexural thermal actuators and their current passes shown by dotted lines

As the current consumption in the cold arm is not necessary, the power efficiency of the actuators can be improved by adding a second hot arm [24]. A double hot arm actuator can have hot arms with the equal or unequal length. Figure 1 shows the current path in the double hot arm actuator and the U-shape actuator (single hot arm actuator).

Most of the thermophysical properties of polysilicon are temperature and process dependent, making complete and accurate modeling very challenging. Mathematical modeling [11, 24–29] and finite element simulations [11] are widely used in MEMS to provide temperature and stress distributions and are also very useful in device optimization (Lin and Chiao [25], Huang and Lee [26–28], Lott et al. [29], Yan et al. [24]). Modeling the thermal actuators involves the three-dimensional (3-D) shape and effect of thermal conduction through the air to the substrate. An electrothermomechanical model of polysilicon thermal actuators in finite element commercial software ABAQUS is presented here. Electrothermomechanical modeling is a sequential and uncoupled procedure. In the first step, an electrothermal model is built to obtain the temperature distribution of the actuator under electrical loading. The obtained temperature distribution is then applied to a thermomechanical model to attain the stress and deformation distributions. Figure 2 shows the geometry of a U-shape actuator used in this modeling. The modeling procedure is explained for a typical U-shape thermal actuator, and the results were validated based on its

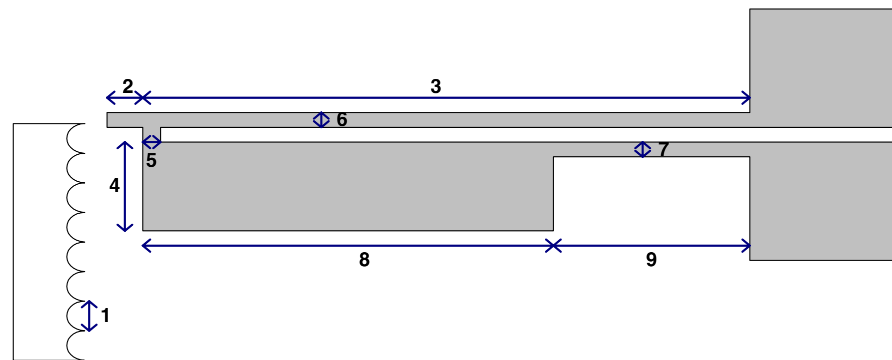

Fig. 2 Dimensions of the actuator (the serrated vernier is for tip-deflection measurement)

	1	2	3	4	5	6	7	8	9
μm	5.76	3.94	200	13.96	2.12	2.42	2.73	162.06	38.24

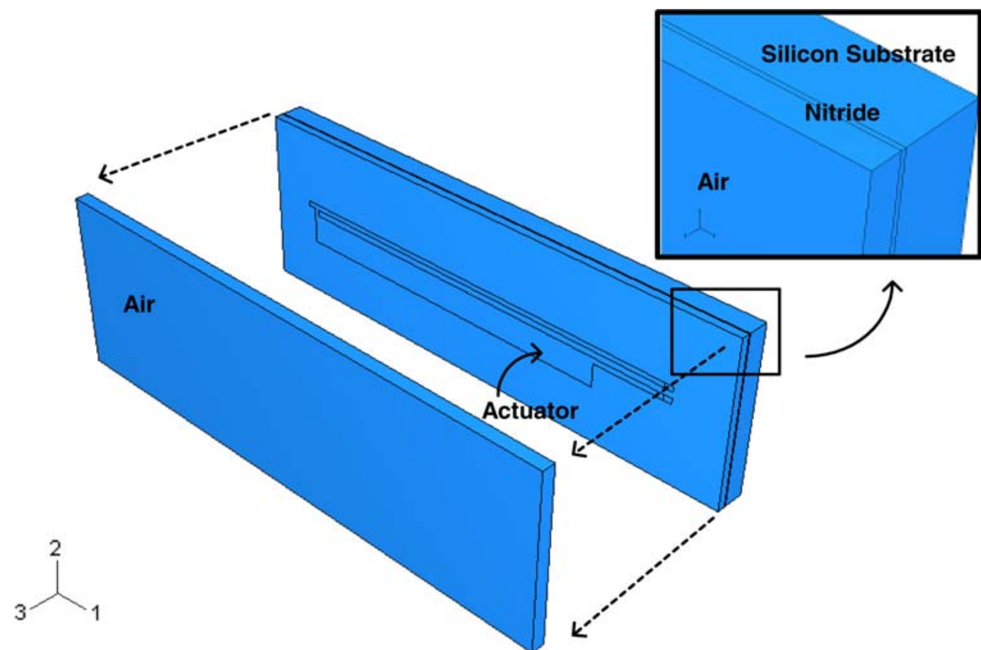

Fig. 3 Actuator and surrounding environment modeling

experimental result. The same procedure is followed for the double hot arm thermal actuators.

While conduction and convection heat transfers are both modeled; radiation effects are ignored because of the small dimension of the hot spot in the actuator. Because of the large mass of the silicon substrate compared with the specimen, temperatures at the end of the actuator were assumed to be constant and equal to the ambient and substrate temperature. A large portion of heat is transferred through the gap between actuator and substrate. To account for this, the surrounding environment (substrate and air) are modeled as solid parts and the interaction with the thermal actuator was maintained through use of proper boundary conditions (Fig. 3). The substrate consists of two 0.6 μm silicon nitride and 10 μm single-crystalline silicon layers. The thickness and dimensions of air and the substrate are large enough to act as an infinite environment.

Material properties of MEMS materials are mostly process dependent [19]. Thermal conductivity and the thermal expansion coefficient of polysilicon are temperature dependent and given in Table 1. The thermal conductivity of air and single crystalline silicon are 0.026E−6 [24] and 148E−6 W/μm °C, respectively. The electrical conductivity of polysilicon is given by Eq. 1. The air, single-crystalline silicon, and silicon nitride were molded as isolators by defining very low electrical conductivity. Young's modulus and Poisson's ratio of polysilicon are 162 GPa and 0.22, respectively. Convection coefficient of air is 5E−11 W/μm^2 °C [24], and the substrate and room temperature are taken to be 20 °C.

The electrical conductivity is related to the resistivity ρ and the temperature:

$$\rho = \rho_0[1 + \xi(T - T_s)] \quad \text{(Eq 1)}$$

where ρ_0 is resistivity of polysilicon at the room temperature, T_s is the environmental temperature, and ξ is a constant equal to 1.25×10^{-3} °C^{-1} [24].

The convection coefficient is also a temperature-dependent parameter. However, the effect is negligible because of the large outer side of the air part.

The anchor effects were implemented by applying constant temperature at the end of the arms in the electrothermal model and fully constrained boundary condition for the thermomechanical model.

Brick elements were used in the actuator and substrate meshing with triangular elements for the air parts. In the environment meshing, finer meshes were used on the surfaces and areas that were in close contact with the actuator. Figure 4 shows temperature contour in the actuator under 4.5 V applied voltage.

Maximum temperature was 580 °C, and the hot spot zone was in the middle of the hot arm which was the narrowest part. The zone was far away from the anchors (which have the room temperature 20 °C) and the cold arm (with around 300 °C). As can be seen, the temperature of the actuator in hot spot was slightly lower in the substrate side because the main heat transfer occurred between the actuator and the substrate through a narrow 2 μm of air.

Table 1 Temperature dependent properties of polysilicon

Temperature, °C	Thermal conductivity [30], W/μm °C	Thermal expansion coefficient [27], °C^{-1}
20	146E−6	2.568E−6
120	98.3E−6	3.212E−6
220	73.2E−6	3.594E−6
320	57.5E−6	3.831E−6
420	49.2E−6	3.987E−6
520	41.8E−6	4.099E−6
620	37.6E−6	4.185E−6
720	34.5E−6	4.258E−6
820	31.4E−6	4.323E−6
920	28.2E−6	4.384E−6

Figure 5 presents the temperature distribution in the actuator beams.

Figure 6 shows the distribution of the von Mises stress for the actuator under 4.5 V load. The highest Mises stress in the actuator was 147 MPa which happened in the "via" part of the actuator away from the hot zone area [4]. The stress at the hot spot was 36.6 MPa. Figure 7 shows the deflection of the actuator under applied voltage.

To validate the FEM results, a series of experiments were conducted on a U-shape thermal actuator with the same dimensions as the model. The tip-deflection measurements are plotted in Fig. 8 and are compared with the FEM results. The solid line represents the results of the model, and the experimental results are shown with the bold square points. The experimental and modeling results are in very good agreement in a wide range of voltage applications. The same modeling procedure and the same material properties were applied to model the two types of double hot arm actuators under consideration.

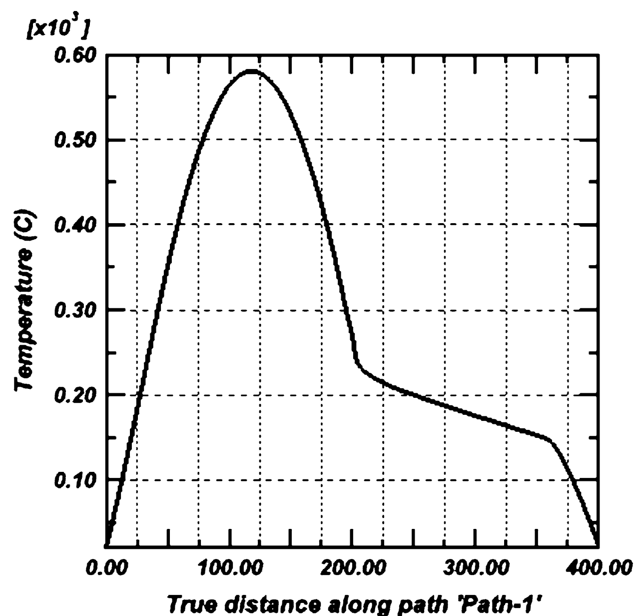

Fig. 5 Temperature distribution along the actuator length. The path begins from the hot arm anchor and ends in the flexure's anchor (see Fig. 1 for definition of path 1)

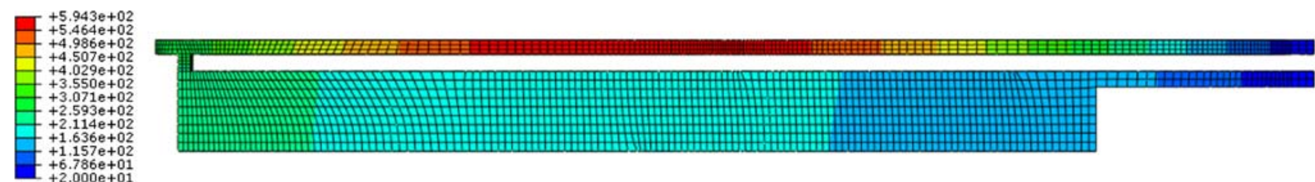

Fig. 4 Temperature distribution (in °C) under 4.5 V loading

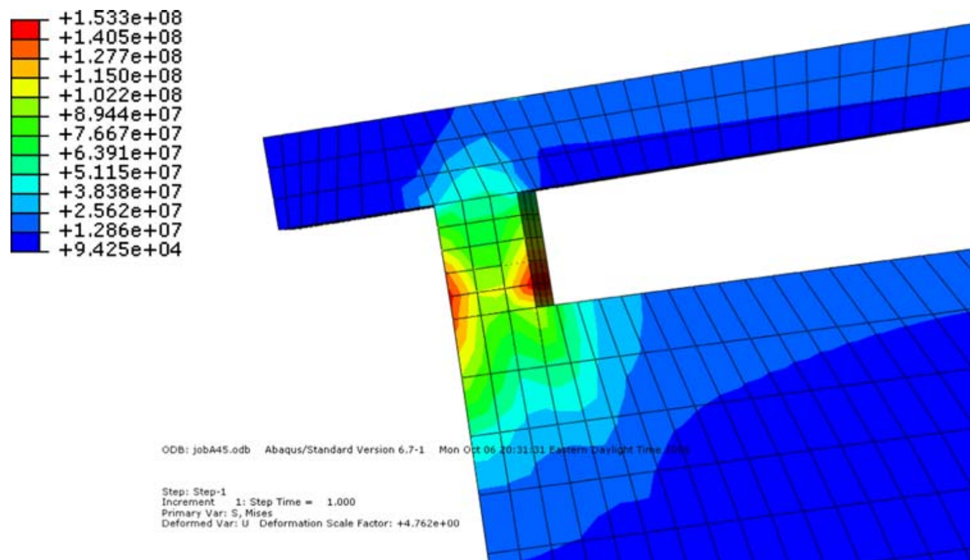

Fig. 6 Von Mises stress (in Pa) at the high stress spot (via section) of the actuator under 4.5 V loading

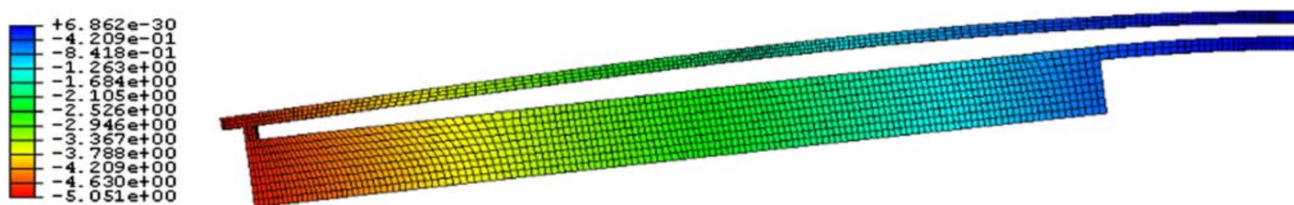

Fig. 7 Deflection of the actuator (in μm) under 4.5 V input voltage

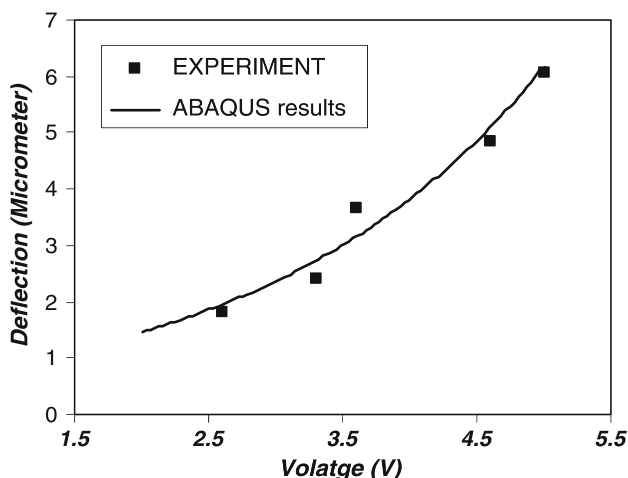

Fig. 8 Comparison of FEM results with the experiment results for the U-shape actuator

Failure Mechanism

Two sets of experiments were conducted on U-shape and double hot arm actuators to find the failure mechanism of the thermal actuators. First, U-shape thermal actuators underwent a fatigue test. In the second set, a number of U-shape and double hot arm actuators were examined for creep failure.

Fatigue

The FE results showed a maximum stress of about 150 MPa in the U-shaped actuator under 4.5 V. Considering the ultimate strength for polysilicon at the microlevel (which has been reported to be around 4 GPa and endurance of about 2 GPa [13]), the stress level is very low and hence should not cause fatigue failure [4]. To confirm this, a fatigue test was conducted on a U-shaped thermal actuator. The thermal actuator was under voltage loading with proper frequency. The chip of the actuator was bound to a DIP package, and the voltage was applied on the pads of the actuator. A 4.5 V input was applied to the actuator anchor with 50 HZ frequency with proper probes, and the test was performed under a microscope during the experiment. The real-time simulation of Simulink/Matlab linked to Wincon3.0.2a was used. MultiQ-3 data acquisition card [31] provided the connection to the real time. At regular intervals, the deflection of the actuator under a constant 4.5 V load was measured. After millions of loading cycles, no change in the deflection was observed. According to the

measured deflection and resistance of the actuator, the actuator had infinite life under fatigue loading with no sign of degradation. Fatigue tests at higher voltages were not carried out since the levels of stress in all cases (which are discussed in the section on creep tests) are well below the endurance limit.

Creep

The experiments were conducted under a microscope to monitor and measure the changes in the tip deflection of the

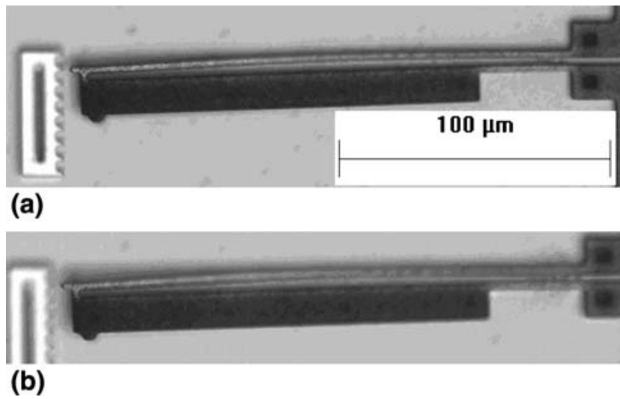

Fig. 9 Creep experiment on a U-shape actuator under 5.2 V. Pictures captured at (**a**) 30 min and (**b**) 192 min of the experiment. Note considerable out-of-plane deflection of the actuator

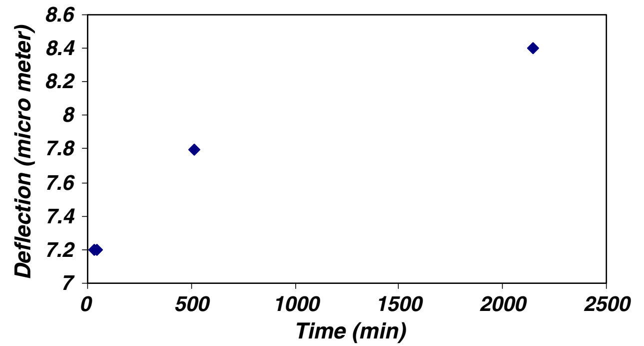

Fig. 10 Tip deflection versus time for the U-shape actuator under 5.2 V in creep tests

Fig. 11 Temperature and bending stress distribution of the unequal double hot arm actuator under 9.3 V

actuator. The FEM model was used to find the voltage level, based on the desired temperature level of each experiment. Creep experiments at different levels of voltages, temperatures, and stresses were conducted on both U-shape and double hot arm actuators.

A U-shape actuator was loaded under 4.5 V with hot spot temperature of 580 °C. The first 3 h of the creep experiment were done under the microscope, and every 10 min a picture was captured. During this time, no measurable tip deflection was observed. The experiment was continued for 3 days, and no significant change was observed.

The second U-shape thermal actuator was loaded under 5.2 V. Temperature and stress level at the hot spot were 850 °C and 74 MPa, respectively. The experiment was continued for 36 h. Based on the applied setting, the pictures were captured in shorter intervals during the first hours of the experiment, but the intervals increased after 1 h. Some of the captured pictures of the actuator are shown in Fig. 9. As it can be seen from the pictures, the tip deflection of the actuator increases during the experiment. The measured tip deflections of the actuator versus time are presented in Fig. 10, which shows a clearly increasing trend. However, the increasing values were not significant.

The double hot arm thermal actuators were also tested for creep. The temperature and stress levels were much higher in these actuators, and faster creep rates were observed. An actuator has been tested under 9.3 V with hot spot temperature of 1022 °C. Figure 11 shows the FEM results for the temperature and stress distributions of the actuator.

The test was continued for 39 h. Figure 12 shows the actuator deformation at different time intervals. At the last stage of the actuator failure, the hot arm became very thin, its resistance increased, and consequently it heated under the electrical current more than the other parts. The test

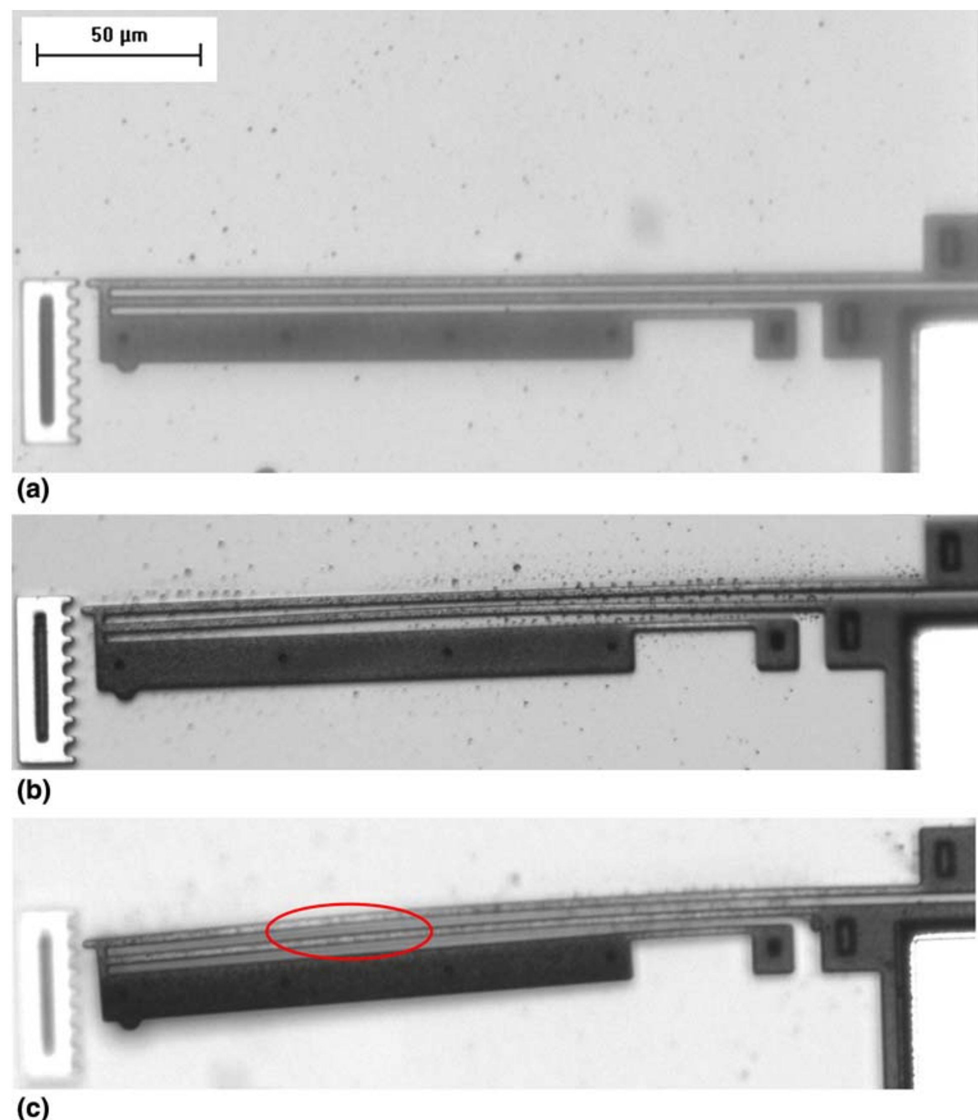

Fig. 12 (**a**) Actuator before the test. (**b**) Initial deflection under 9.3 V. (**c**) Deflection after 17 h of creep test

was stopped at this stage. As shown in Fig. 11, based on the FEM model the stress in the inner hot arm is compressive and high. The highest temperature is 1022 °C and is in the middle arm where the corresponding maximum principal stress is 174 MPa. In this type of double hot arm thermal actuators, the highest temperature and highest stress happen in the same position, which makes the creep rate faster.

The fourth creep test was conducted on an equal-length double hot arm thermal actuator. This test was done under 9.5 V, and the initial deflection of the actuator was 7.22 µm. Figure 13 shows the temperature and stress distributions of the actuator. Figure 14 shows the actuator in the different levels of the creep test. Figure 15 shows images captured after 100 min and up to 370 min into the testing. In Fig. 15a, the distance between the two hot arms

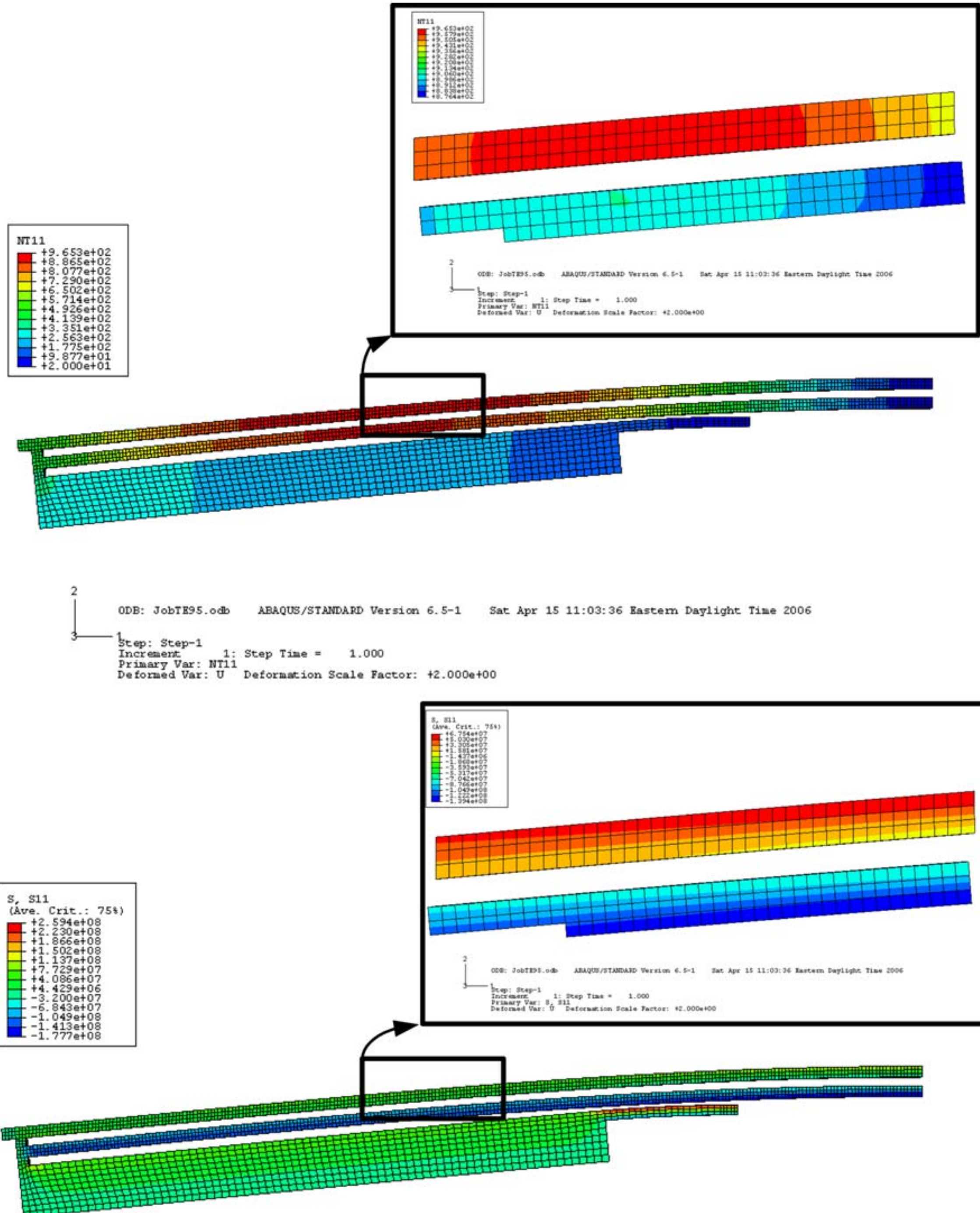

Fig. 13 Stress and temperature distribution in the equal double hot arm actuator under 9.5 V

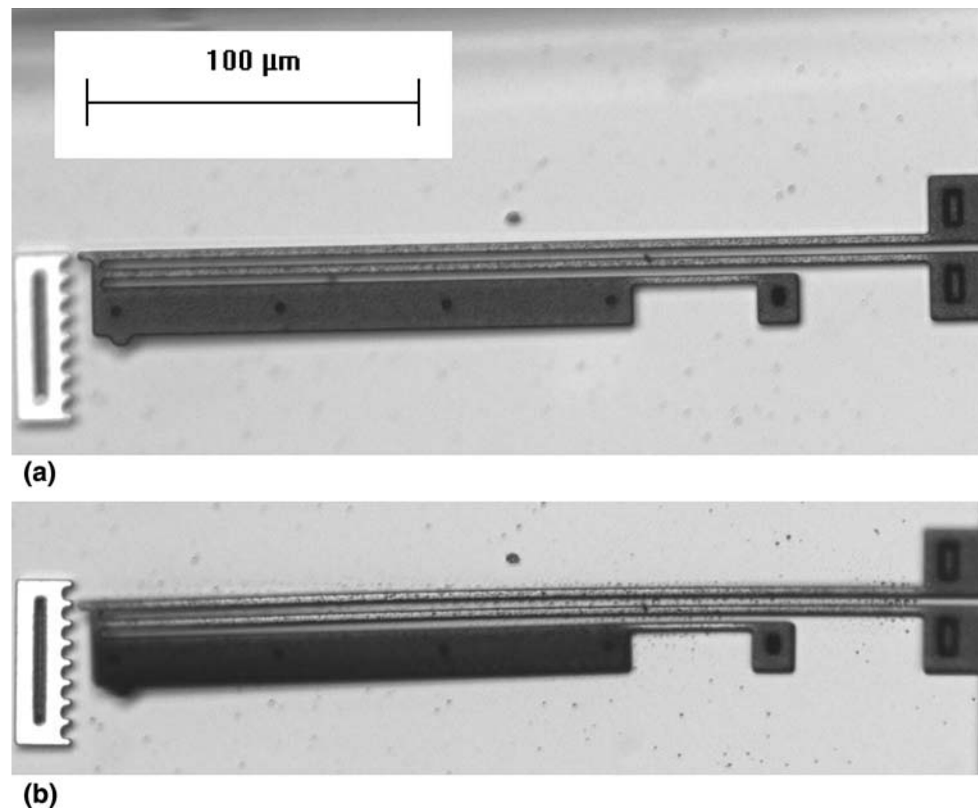

Fig. 14 A double hot arm actuator in creep test under 9.5 V, (**a**) initial deflection, and (**b**) after 15 min

increased in the circled area. The tip deflection of the actuator gradually increased. The experiment was stopped after 6 h of the creep experiment in 370 min.

As shown in Fig. 13, the highest temperature in the actuator is 965 °C, and it is located at the outer hot arm. The maximum principal stress on the hot spot is 63 MPa. However, the stress at the inner hot arm, where temperature is 910 °C, is 136 MPa. Since the highest temperature and stress positions were not the same, a slower creep trend was expected for this type of double hot arm actuator compared with the unequal-length double hot arm actuators.

The deflection–time curve of the thermal actuators is plotted in Fig. 16. The actuator showed a typical three-stage creep curve. The accuracy of the deflection measurement was ±0.3 μm.

Discussion

Finite element modeling gives an insight into the stress and temperature distributions in MEMS devices. In this study, a modeling approach was used and validated by experimental results. In addition, the actuators were examined by fatigue and creep tests.

A U-shape actuator was tested under fatigue loading and did not show any effect of degradation or failure due to the cyclic load. The observed results were consistent with the studies in the literature stating that fatigue is not a feasible failure mechanism in polysilicon MEMS thermal actuators under operational load. However, in creep tests, eventually all the actuators permanently deflected, and failed, showing that creep is a viable failure mechanism in these thermal actuators.

Several types of the actuators were studied in the creep experiments of U-shape and double hot arm thermal actuators. Two types of double hot arm thermal actuators were tested, equal-length and unequal-length hot arms, which have different stress and temperature distribution profiles. Based on the temperature and stress distribution obtained from the finite element modeling, the highest temperature and stress for equal-length double hot arm thermal actuators were not at the same location (hot spot was at outer hot arm, but maximum principal stress was at the inner hot arm). On the other hand, the hot spot and the highest stress in unequal-length thermal actuators were at the same position (at inner hot arm), causing faster creep deformation. The difference in the creep life is also observed in the double hot arm actuators. It was observed that the permanent deformation in unequal-length thermal actuator started after 1020 min, while under same conditions the same permanent deformation was observed after 215 min in equal-length actuator under the same input voltage (9.3–9.5 V).

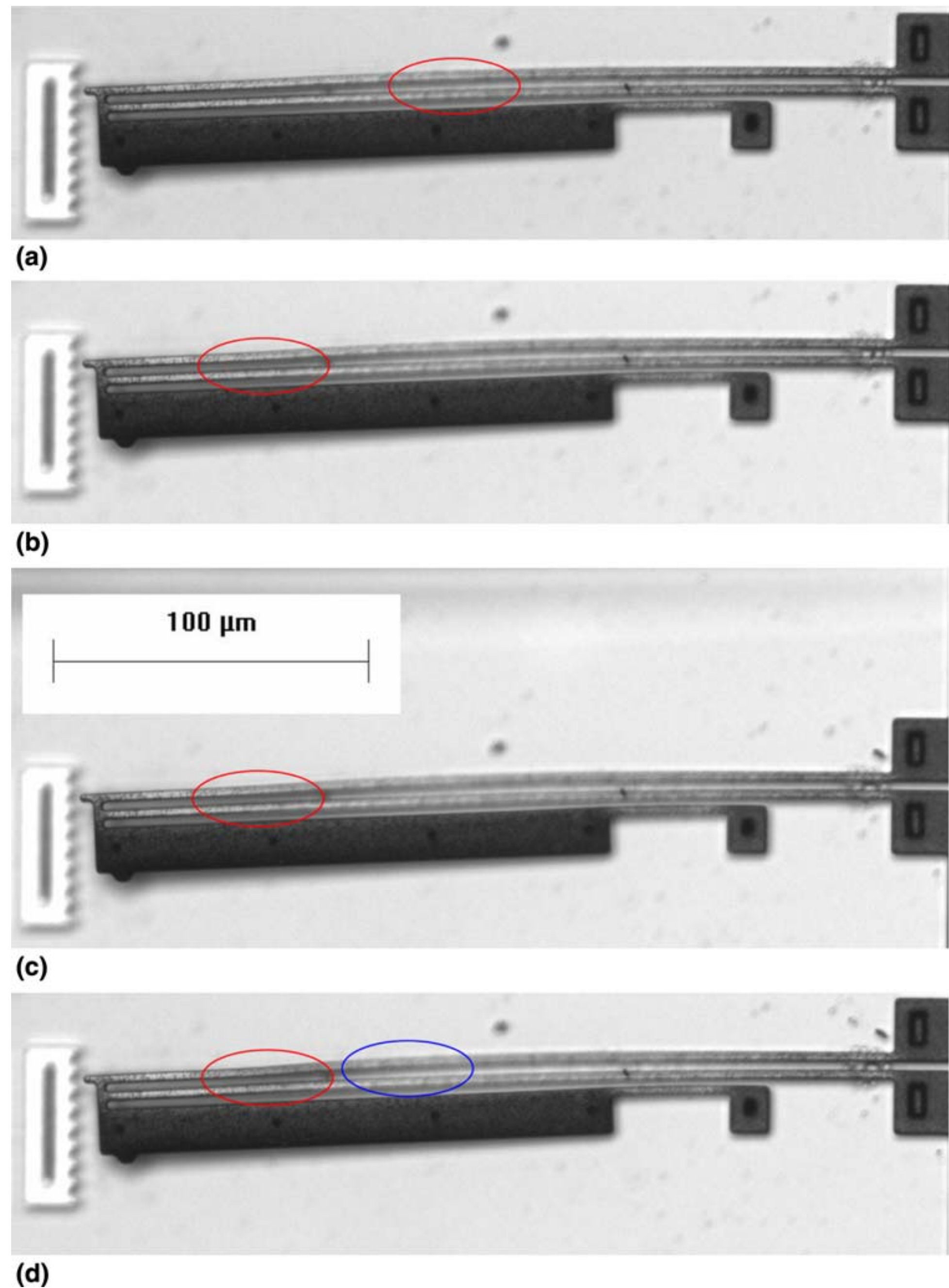

Fig. 15 Actuator in creep test under 9.5 V after (**a**) 100 min, (**b**) 165 min, (**c**) 215 min, and (**d**) 370 min

The permanent deformation on the equal-length double hot arm actuator occurred near the tip of the actuator. During the experiment the thickness of the outer hot arm decreased, leading to a sudden increase of temperature. The permanent plastic deformation happened at the exact same point. This may be the result of the degradation of yielding stress of the material caused by the high temperature. The strength level fell below this level, and the structure deformed plastically. The observation after relaxation time showed that no recovery occurred at this point.

All actuators had deflected in both in-plane and out-of-plane directions. The tendency of the actuators to deflect out of the plane may be caused by the microstructure defects induced by the fabrication process. This mode of deflection was not expected in the actuators because they were fabricated based on a symmetric structure design. However, the experiment showed that the condition was not symmetric across the beam thickness and the tendency to deflect out-of-plane was high.

From the results, the three common stages of creep behavior were observed in thermal actuators. The strain

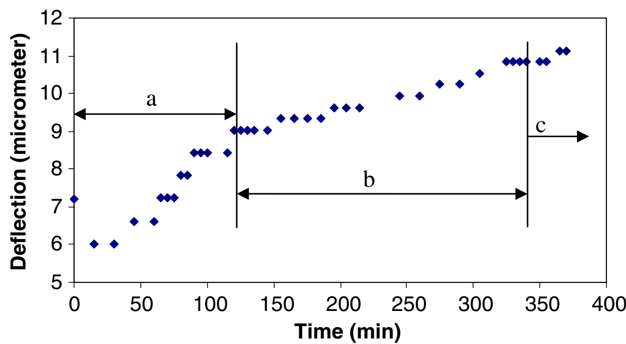

Fig. 16 Deflection–time curve of the thermal actuator under the creep experiment

versus time curve shown in Fig. 16 consists of three regions. The primary creep stage "a" with slight decreasing creep rate, the secondary (and much longer) creep stage "b" with constant creep rate, and the tertiary creep stage "c" with acceleration of creep rate that ultimately leads to failure.

Conclusion

The experimental data and analyses presented in this paper show that the MEMS thermal actuator did not failed because of fatigue. A series of the creep experiments were conducted on MEMS thermal actuators (U-shape and double hot arm thermal actuators). Captured images and the deformation trend on the actuators were presented. The deflection–time curves based on the accurate tip-deflection measurements of the actuators are presented, which show a typical three-stage shape.

All the tested thermal actuators showed time-dependent deformation under stresses and high-temperature conditions. They also experience some level of plasticity caused by material degradation effects at high temperatures. In addition, the creep lifetime of the actuator in which high temperature and high stress are in the same location is less than in the other actuators under the same level of applied voltage. These results demonstrate that creep is both a viable and dominant failure mechanism for the MEMS device considered.

Acknowledgment The authors would like to acknowledge the financial support of the Natural Sciences and Engineering Research Council of Canada (NSERC).

References

1. Guckel, H., Kelan, J., Christenson, T., Scrobis, K., Laudon, M., Lovell, E.G.: Thermo-magnetic metal flexure actuator. In: IEEE Solid-State Sensor and Actuator Workshop, pp. 73–75 (1992)
2. Comtois, J.H., Bright, V.M.: Application for surface-micro machined poly silicon thermal actuators and arrays. J. Sensors Actuators A **58**, 19–25 (1997)
3. Burns, D.M., Bright, V.M.: Design and performance of a double hot arm polysilicon thermal actuator. SPIE **3224**, 296–305 (1997)
4. Conant, R., Muller, R.S.: Cyclic fatigue testing of surface-micromachined thermal actuators. In: Proc. ASME International Mechanical Engineering Congress and Exposition, vol. 66, pp. 273–277 (1998)
5. Tuck, K., Jungen, A., Giesberger, A., Ellis, M., Skidmore, G.: A study of creep in polysilicon MEMS devices. J. Eng. Mater. Technol. **127**, 90–96 (2005)
6. Fukutta, Y., Collard, D., Akiyama, T., Yang, E.H., Fujita, H.: Microactuated self-assembling of 3D polysilicon structures with reshaping technology. In: Proc. IEEE 10th Annual International Workshop on MEMS, pp. 477–481 (1997)
7. Teh, K.S., Lin, L.: Time-dependent buckling phenomena of polysilicon micro beams. J. Microelectron. **30**, 1169–1172 (1999)
8. Judy, J.W., Tamagawa, T., Polla, D.L.: Surface micromachined linear thermal actuator. In: Proc. 1990 IEEE International Electro Devices Meeting, pp. 629–632 (1990)
9. Sharpe Jr, W.N.: Tensile testing at micrometer scale: opportunities in experimental mechanics. J. Exp. Mech. **43**, 228–238 (2003)
10. Oh, C.S., Sharpe Jr, W.N.: Techniques for measuring thermal expansion and creep of polysilicon. J. Sensors Actuators A **112**, 66–73 (2004)
11. Paryab, N., Jahed, H., Khajepour, A.: Failure mechanisms of MEMS thermal actuators. In: Proc. ASME International Mechanical Engineering Congress and Exposition, Chicago, IL (2006)
12. Brown, S.B., Arsdell, W.V., Muhlstein, C.L.: Materials reliability in MEMS devices. In: IEEE International Conference on Solid-State Sensors and Actuators (1997)
13. Muhlstein, C.L., Brown, S.B., Ritchie, R.O.: High-cycle fatigue and durability of poly crystalline silicon thin films in ambient air. Sensors Actuators A **94**, 177–188 (2001)
14. Comtois, J.H., Michalicek, M.A., Barron, C.C.: Electro thermal actuators fabricated in four-level planarized surface micro machined polycrystalline silicon. Sensors Actuator A **70**, 23–31 (1998)
15. Kapels, H., Aigner, R., Binder, J.: Fracture strength and fatigue of poly silicon determined by a novel thermal actuator. IEEE Trans. Electron. Dev. **47**(7), 1522–1528 (2000)
16. Que, L., Park, J.-S., Li, M.-H., Gianchandani, Y.B.: Reliability studies of bent-beam electro-thermal actuators. In: IEEE Annual International Reliability Physics Symposium, pp. 118–122 (2000)
17. Chen, W.-C., Hsieh, J., Fang, W.: A novel single layer bi-directional out-of-plane electro thermal micro actuator. In: IEEE, pp. 693–697 (2002)
18. Chen, W.-C., Chu, C.-C., Hsieh, J., Fang, W.: A reliable single-layer out-of-plane micro machined thermal actuator. Sensors Actuators A **103**, 48–58 (2003)
19. Hocheng, H., Kao, K.S., Fang, W.: Fatigue life of a micro cantilever beam in bending. J. Vac. Sci. Technol. B **22**(6), 3143 (2004)
20. Kung, C., Chen, R.C.: Fatigue analysis of U-shaped flexural electro-thermal micro-actuators. J. Chin. Inst. Eng. **28**(1), 123–130 (2005)
21. Ritchie, R.O., Muhlstein, C.L., Nalla, R.K.: Failure by fracture and fatigue in nano and bio material. JSME Int. J. A **47**(3), 238–251 (2004)
22. Alsem, D.H., Stach, E.A., Muhlstein, C.L., Ritchie, R.O.: Fatigue failure in thin-film polycrystalline silicon is due to sub critical cracking with in the oxide layer. Appl. Phys. Lett. **86**, 041914 (1–3) (2005)

23. Kahn, H., Huff, M.A., Heuer, A.H.: Heating effects on the Young's modulus of films sputtered on to micro machined resonators. In: Material Research Society Symposium Processing, vol. 518, pp. 33–38 (1998)
24. Yan, D., Khajepour, A., Mansour, R.: Modeling of two-hot-arm horizontal thermal actuator. J. Micromechan. Microeng. **13**, 1–11 (2003)
25. Lin, L., Chiao, M.: Electrothermal responses of lineshape microstructures. J. Sensors Actuators **55**, 35–41 (1996)
26. Huang, Q.-A., Lee, N.K.S.: Analysis and design of polysilicon thermal flexure actuator. J. Micromechan. Microeng. **9**, 64–70 (1999)
27. Huang, Q.-A., Lee, N.K.S.: Analytical modeling and optimization for a laterally driven polysilicon thermal actuator. J. Microsyst. Technol. **5**, 133–137 (1999)
28. Huang, Q.-A., Lee, N.K.S.: A simple approach to characterizing the driving force of polysilicon laterally driven thermal microactuators. J. Sensors Actuators **80**, 267–272 (2000)
29. Lott, C.D., McLain, T.W., Harb, J.N., Howell, L.L.: Thermal modeling of surface-micromachined linear thermomechanical actuator, In: Technical Proceedings of the Fourth International Conference on Modeling and Simulation of Microsystems, MSM 2001, Hilton Head Island, SC, pp. 370–373 (Mar 2001)
30. Mankame, N., Ananthasuresh, G.K.: Comprehensive thermal modelling and characterization of an electro-thermal-compliant micro actuator. J. Micromechan. Microeng. **11**, 452–462 (2001)
31. MultiQ-3TM programming manual. http://www.memscap.com/memsrus/docs/polymumps.dr.v10.pdf